



Phenotypic Reprogramming of Striatal Neurons into Dopaminergic Neuron-like Cells in the Adult Mouse Brain

Wenze Niu,^{1,2,3} Tong Zang,^{1,2} Lei-Lei Wang,^{1,2} Yuhua Zou,¹ and Chun-Li Zhang^{1,*}

¹Department of Molecular Biology, Hamon Center for Regenerative Science and Medicine, University of Texas Southwestern Medical Center, 6000 Harry Hines Boulevard, Dallas, TX 75390, USA

²Co-first author

³Present address: College of Osteopathic Medicine of the Pacific Western University of Health Sciences, Pomona, CA 91766, USA

*Correspondence: chun-li.zhang@utsouthwestern.edu

<https://doi.org/10.1016/j.stemcr.2018.09.004>

SUMMARY

Neuronal subtype is largely fixed in the adult mammalian brain. Here, however, we unexpectedly reveal that adult mouse striatal neurons can be reprogrammed into dopaminergic neuron-like cells (iDALs). This *in vivo* phenotypic reprogramming can be promoted by a stem cell factor (SOX2), three dopaminergic neuron-enriched transcription regulators (NURR1, LMX1A, and FOXA2), and a chemical compound (valproic acid). Although the site of action of the reprogramming factors remains to be determined, immunohistochemistry and genetic lineage mappings confirm striatal neurons as the cell origin for iDALs. iDALs exhibit electrophysiological properties stereotypical to endogenous dopaminergic rather than striatal neurons. Together, these results indicate that neuronal phenotype can be reengineered even in the adult brain, implicating a therapeutic strategy for neurological diseases.

INTRODUCTION

Neuron replacement may have medical implications for neural injury and neurological diseases. Except for a few defined niches (Bond et al., 2015; Zhao et al., 2008), however, neuron-producing progenitors do not exist in most regions of the adult mammalian central nervous system. Very interestingly, recent data rather reveal that ectopic SOX2 can reprogram resident glial cells into neural progenitors in both the adult mouse brain and spinal cord (Niu et al., 2013, 2015; Su et al., 2014; Wang et al., 2016; Wang and Zhang, 2018). These induced progenitors expand locally and give rise to mature neurons with network integration.

Resident glial cells in the adult mouse brain or retina can also be directly converted into neurons with ectopic expression of a single or a combination of fate-determining factors. These include *Neurod1*, *Neurog2*, *Olig2*, *Sox2*, *Ascl1*, *Brn2*, *Myt1l*, etc. (Buffo et al., 2005; Chen et al., 2015; Gascon et al., 2016; Grande et al., 2013; Guo et al., 2014; Heinrich et al., 2014; Jorstad et al., 2017; Liu et al., 2015; Pereira et al., 2017; Rivetti di Val Cervo et al., 2017; Smith et al., 2016a; Smith et al., 2016b; Smith and Zhang, 2015; Torper et al., 2015; Torper et al., 2013). Some of these glia-converted neurons show electrophysiological properties of mature neurons and form synaptic connections.

In contrast to glial cells that can become reactive and proliferate under certain conditions, postmitotic neurons do not normally change their identity for the lifespan of the organism. Notwithstanding, ectopic *Fezf2* can switch the subtype of certain early postmitotic neurons in the mouse brain. Such subtype reprogramming is restricted to the first

postnatal week, indicating a critical window of neuronal plasticity (De la Rossa et al., 2013; Rouaux and Arlotta, 2013). In this study, we sought to induce new dopaminergic (DA) neurons through SOX2-mediated cell fate reprogramming *in vivo*. However, we unexpectedly identified that striatal neurons but not glial cells in the adult mouse brain can be induced into a phenotype resembling DA neurons, greatly expanding our knowledge on neuronal plasticity.

RESULTS

Induction of Dopaminergic Neuron-like Cells in the Adult Mouse Striatum

DA neurons are critical for movement coordination and motivated behavior and are frequently lost in Parkinson disease (Lindvall and Bjorklund, 2011; Palmiter, 2008). *In vivo* generation of new DA neurons may have broad applications including therapeutic potentials. We previously showed that ectopic SOX2 could reprogram striatal glia into neural progenitors, which then further became mature neurons when the mice were treated with the small molecule valproic acid (VPA) (Niu et al., 2013, 2015). To determine whether any of these induced neurons were DA neurons, immunohistochemistry was performed by using an antibody against the rate-limiting enzyme for dopamine synthesis, tyrosine hydroxylase (TH). Antibody specificity for TH was verified since it can clearly detect the somas of DA neurons in the substantia nigra pars compacta (SNc) and their projections in the striatum (Figure S1). A systematic survey, however, failed to detect any induced TH⁺ cells

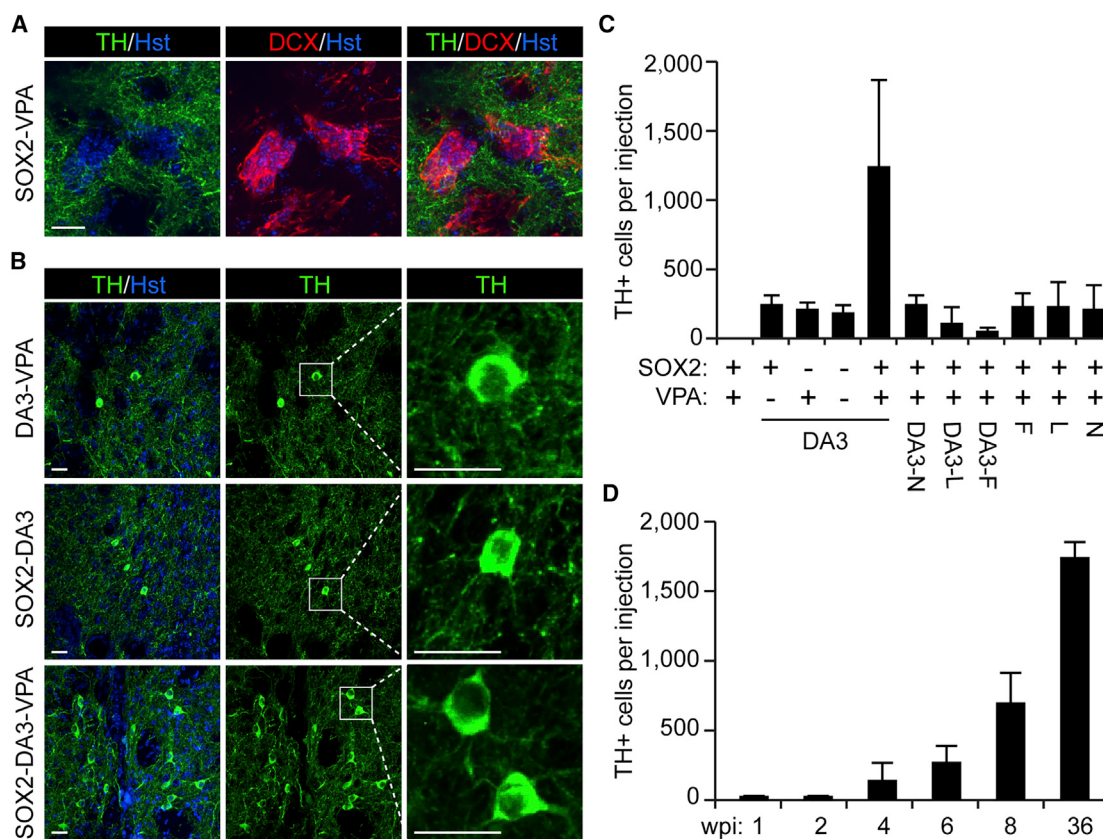


Figure 1. A Combination of Factors Induces iDALs in the Adult Mouse Striatum

(A) *In vivo* reprogramming by SOX2 and VPA is not sufficient for iDALs. TH⁺ somas were not detected in striatal regions injected with SOX2 virus and treated with VPA when analyzed at 8 wpi (weeks post injection of virus; n > 3 mice). Induced DCX⁺ neurons were used as controls for SOX2-dependent *in vivo* reprogramming activity. Cell nuclei were counterstained with Hoechst 33342 (Hst). Scale bar, 20 μm.

(B) Confocal images of iDALs by the indicated factors at 8 wpi. Enlarged views of the boxed regions are also shown. Nuclei were counterstained with Hst. Scale bars, 20 μm.

(C) Quantification of iDALs at 8 wpi (mean ± SD; n = 3 mice per group; group effect by one-way ANOVA: F(10,22) = 7.345 and p < 0.0001). N, NURR1; F, FOXA2; L, LMX1A; DA3, a combination of NURR1, FOXA2, and LMX1A.

(D) A time course analysis of iDALs induced by SOX2+DA3+VPA (mean ± SD; n = 3–4 mice per group; time effect by one-way ANOVA: F(5,14) = 101.7 and p < 0.0001). wpi, weeks post injection of virus.

See also Figures S1 and S2.

in the core striatal regions that were injected with the SOX2-expressing virus, although DCX⁺ cells were clearly observed indicating SOX2-mediated neuronal reprogramming (Figure 1A).

Therefore, we screened additional fate-determining transcription factors that could facilitate SOX2 to induce new TH⁺ cells in the adult striatum. Immunohistochemistry was initially conducted at 8 weeks post injection of virus (wpi). This time point was chosen so that only survived and mature neurons would be detected. Whereas the inclusion of GSX2, DLX2, EBF1, EGR1, or ASCL1 had no any effect, the combination of SOX2 with either FOXA2, LMX1A, or NURR1 induced some striatal cells with TH⁺ somas (Figure S2A). Very interestingly, a larger

number of TH⁺ somas was observed when combining all those factors that showed a positive effect (Figures 1B and 1C; n = 3 mice per group; group effect by one-way ANOVA: F(10,22) = 7.345 and p < 0.0001). These factors include SOX2, three DA neuron-restricted transcription factors (DA3: NURR1, FOXA2, and LMX1A), and the small-molecule VPA. Removing any one of these factors from the combination reduced the number of neurons with TH⁺ somas in the striatum (Figure 1C). For simplicity, this combination of factors is hereafter referred to as iDAL factors, and the induced striatal cells with TH⁺ somas as iDALs.

A time course analysis showed that iDALs were detectable at 2 wpi and their number gradually increased at later time

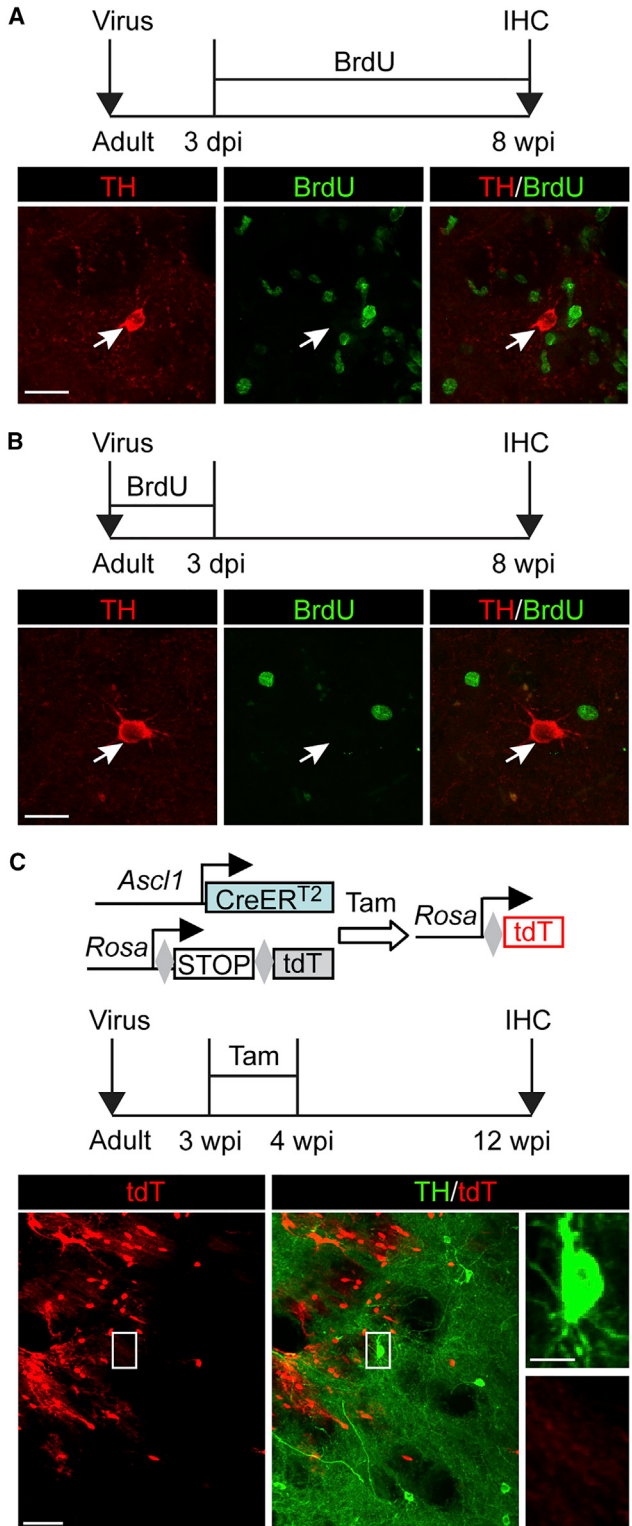


Figure 2. iDALs Do Not Pass through a Proliferative Progenitor Stage

(A and B) iDALs are not traced by BrdU incorporation. Mice were treated with BrdU in drinking water (A) or through twice daily

points (Figure 1D; $n = 3\text{--}4$ mice per group; time effect by one-way ANOVA: $F(5,14) = 101.7$ and $p < 0.0001$). It should be noted that the numbers of iDALs varied between experiments (Figures 1C and 1D). Such quantitative differences might originate from normal variations between independent experiments, such as slight changes on virus quality and titers. Interestingly, induced calretinin (CR)⁺ cells were also observed in the virus-injected striatal regions and they were frequently intermingled with iDALs (Figure S2B). These induced CR⁺ cells were likely due to the reprogramming activity of SOX2 and VPA, as we had shown previously (Niu et al., 2015).

iDALs Do Not Pass through a Proliferative Progenitor Stage

SOX2-mediated *in vivo* reprogramming passes through a proliferative ASCL1⁺ progenitor stage (Niu et al., 2013, 2015; Wang et al., 2016). To determine whether cell proliferation was also involved in iDALs, we systemically treated the mice with either bromodeoxyuridine (BrdU)-containing drinking water (Figure 2A) or through twice daily intraperitoneal BrdU injections (Figure 2B). These BrdU treatments covered all the time periods immediately after virus injections until analysis by immunohistochemistry at 8 wpi. iDALs were examined by immunostainings of TH and BrdU. Unexpectedly, none of the iDALs were co-labeled with BrdU (Figures 2A and 2B; $n = 0$ BrdU⁺TH⁺ cells from a total of six mice).

SOX2-induced neural progenitors and their progenies in the adult striatum could be traced in *Ascl1-CreER^{T2}; Rosa-tdTomato (tdT)* mice (Niu et al., 2015). The reporter tdT was induced by treating the mice with tamoxifen (Tam) at 3 wpi. Cell fate was analyzed at 12 wpi (Figure 2C). Consistent with our previous results (Niu et al., 2015), tdT⁺ neurons were induced in striatal regions injected with the reprogramming factors (Figure 2C). However, none of the TH⁺ iDALs were labeled by tdT in the same striatal region (Figure 2C; $n = 0$ tdT⁺TH⁺ cells from a total of four mice). Together, these results indicate that iDALs are directly induced from non-proliferative cells and do not originate from SOX2-induced or any endogenous ASCL1⁺ neural progenitors.

intraperitoneal injections (B) for the indicated durations. Representative confocal images are shown ($n = 0$ BrdU⁺TH⁺ cells from three mice at each condition). dpi, days post injection of virus; wpi, weeks post injection of virus; IHC, immunohistochemistry. Scale bars, 20 μ m.

(C) iDALs do not pass through a progenitor state. Induced neural progenitors were traced in *Ascl1-CreER^{T2}; Rosa-tdT* mice after tamoxifen (Tam) injections ($n = 0$ tdT⁺TH⁺ cells from a total of four mice). Scale bars, 50 μ m (in lower magnification view) and 10 μ m (in higher magnification view).

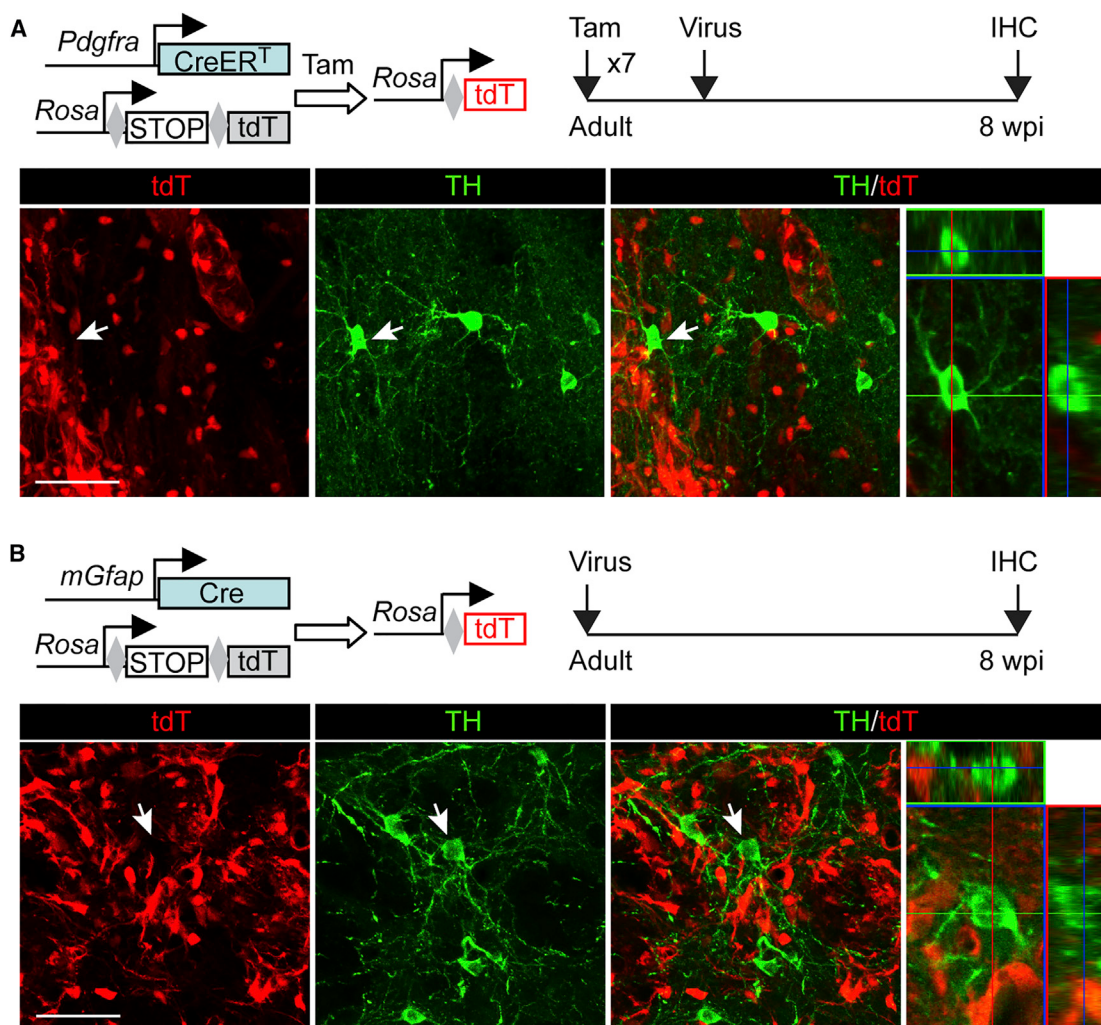


Figure 3. Glial Cells Are Not a Cell Origin for iDALs

(A) iDALs do not come from resident NG2 glia. NG2 glia and their derivatives were traced in *Pdgfra-CreERT;Rosa-tdT* mice after Tam injections. Representative confocal images show that TH⁺ iDALs are not traced by the reporter tdT ($n = 0$ tdT⁺TH⁺ cells from three mice). Scale bar, 50 μ m.

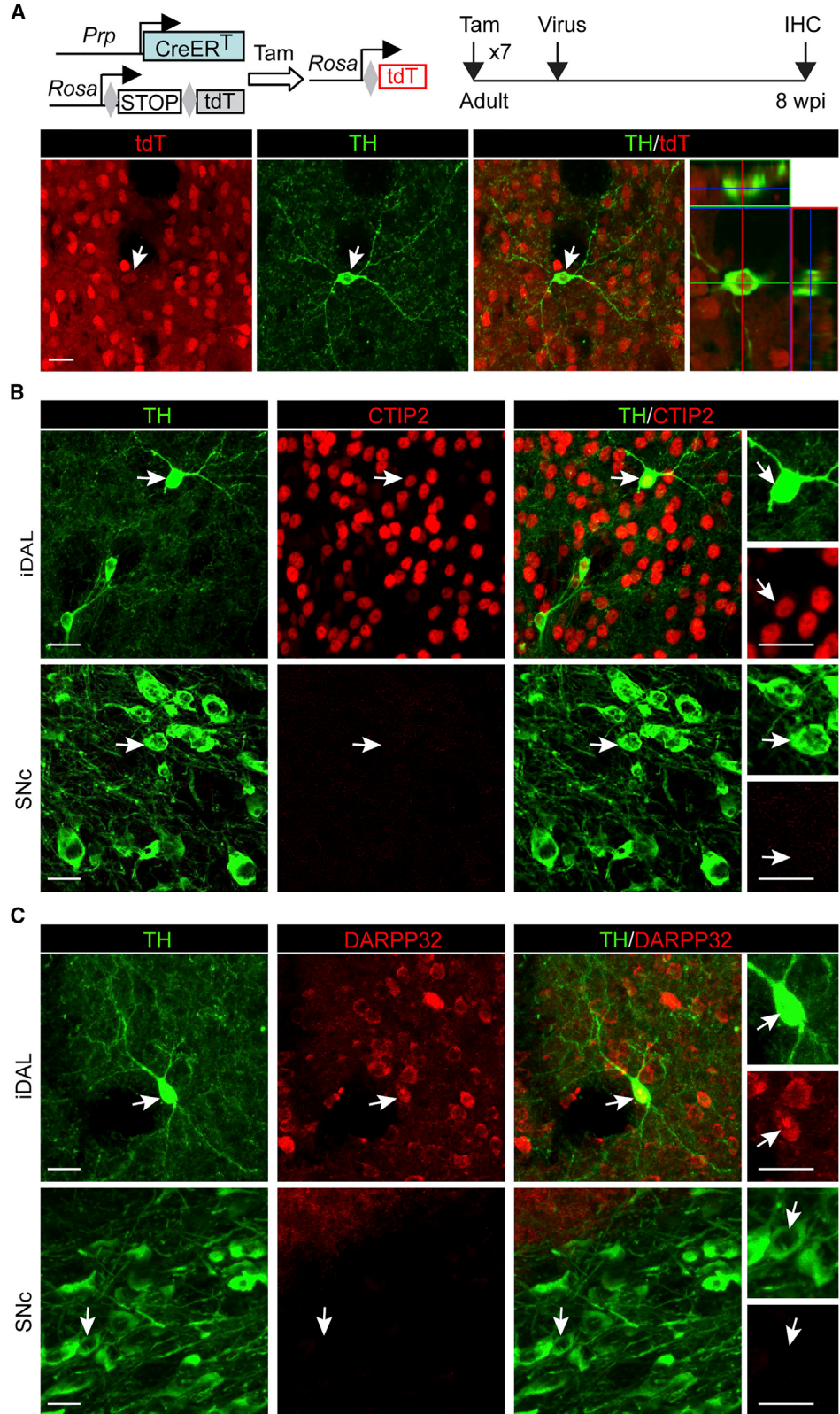
(B) iDALs do not come from resident astrocytes. Astrocytes and their derivatives were traced in *mGfap-Cre;Rosa-tdT* mice. Representative confocal images show TH⁺ iDALs are not traced by the reporter tdT ($n = 0$ tdT⁺TH⁺ cells from three mice). Scale bar, 50 μ m. See also Figures S3 and S4.

iDALs Do Not Originate from Resident Glial Cells or Progenitors in the Subventricular Zone

Resident astrocytes or NG2 glia can be reprogrammed into neurons (Guo et al., 2014; Heinrich et al., 2014; Niu et al., 2013; Pereira et al., 2017; Torper et al., 2013, 2015). We used the *Pdgfra-CreERT;Rosa-tdT* mice to trace NG2 glia and their lineages (Kang et al., 2010). Permanent reporter expression in NG2 glia was induced through Tam administration in the adult mice (Figure 3A). iDALs were determined by immunostaining of TH⁺ somas in the virus-injected striatal region at 8 wpi. Interestingly, none of the iDALs were labeled by the reporter tdT ($n = 0$ tdT⁺TH⁺ cells

from three mice), indicating that iDALs do not come from resident NG2 glia.

The *mGfap-Cre;Rosa-tdT* transgenic mouse line was then employed to genetically trace astrocytes and their converted neurons (Niu et al., 2013). Approximately 98% of the striatal astrocytes was shown to be traced in this line (Niu et al., 2013). In addition to astrocytes, neural progenitors in the subventricular zone could also be labeled in this Cre line (Figure S3) (Gregorian et al., 2009). Adult transgenic mice were injected with iDAL factor-expressing virus and treated with VPA (Figure 3B). iDALs were then examined for expression of TH and tdT at 8 wpi. Very



(legend on next page)



unexpectedly, none of the TH⁺ iDALs were labeled by the reporter tdT, even though they were intermingled with tdT⁺ astrocytes in the same striatal region (Figure 3B; n = 0 tdT⁺TH⁺ cells from three mice). Low-magnification images also showed that iDALs were found in injected striatal regions far away from the subventricular zone (Figure S4), excluding the likelihood that iDALs could be originated from this neurogenic zone through cell migration. Together, these results clearly indicate that neither resident glial cells nor neural progenitors in the neurogenic subventricular zone are a cell source for iDALs.

iDALs Originate from Local Striatal Neurons

We finally postulated that iDALs might come from local neurons through phenotypic reprogramming. To temporally trace neurons and their derivatives, we used the Tam-inducible *PrP-CreER^T;Rosa-tdT* reporter mice (Niu et al., 2013). Approximately 80% of preexisting striatal neurons could be permanently labeled by repetitive Tam injections once per day for 7 days (Figure S5A). The adult reporter mice were then injected with virus expressing the iDAL factors and treated with VPA in drinking water. When analyzed at 8 wpi, about 79% of iDALs were found to be labeled by tdT⁺, indicating that they came from endogenous striatal neurons (Figures 4A and S5B; n = 206 tdT⁺TH⁺ cells out of 259 TH⁺ cells from three mice).

Immunohistochemistry was further conducted to examine marker expression for medium spiny neurons (MSNs), which are the predominant neuronal subtype in the striatum (Arlotta et al., 2008). These neurons can be identified by expression of DARPP32 (dopamine- and cAMP-regulated neuronal phosphoprotein) and CTIP2 (also known as BCL11b) (Arlotta et al., 2008). Very interestingly, these two markers were clearly detectable in iDALs (Figures 4B and 4C). Such a staining pattern was in sharp contrast to those endogenous DA neurons in the SNc, which completely lacked the expression of these two markers. Collectively, these data indicate that iDALs come from local striatal neurons.

We then examined whether striatal MSNs had the viral SOX2 expression, since it was driven by the *hGFAP* promoter that mainly targets resident astrocytes (Lee et al., 2008). We used the *hGFAP-GFP-T2A-SOX2* lentivirus to express SOX2 and *hGFAP-GFP* as a control. Endogenous striatal neurons were detected by DARPP32 and CTIP2. Consistent with our previously published data (Niu et al., 2013),

the result showed that about 10% of the striatal neurons could be transduced by the lentivirus in addition to a majority of astrocytes (Figure S6A). The GFP-SOX2 was then used in combination with DA3 factors to induce iDALs in the adult mouse striatum. Interestingly, not all TH⁺ iDALs were marked by GFP-SOX2 (Figure S6B), which might be consistent with the results that iDALs could also be induced in the absence of SOX2 (Figures 1B and 1C). It could also be possible that GFP-SOX2 is downregulated in some iDALs or that the reprogramming factors might have non-cell-autonomous effects on the appearance of iDALs. The site of action of the reprogramming factors remains to be determined.

iDALs Express Markers Stereotypical to DA Neurons

The detection of markers for striatal neurons in iDALs raised a possibility that these neurons might merely express TH but lack of other properties typical to functional DA neurons. As such, we examined additional subtype-specific markers. Dopa decarboxylase (DDC), also known as aromatic L-amino acid decarboxylase, is a key downstream enzyme of TH that is required for dopamine synthesis. Membrane-bound vesicular monoamine transporter 2 (VMAT2) is critical for transporting dopamine into synaptic vesicles. On the other hand, the membrane-spanning dopamine transporter (DAT) controls dopamine reuptake from the synaptic cleft. TH⁺ iDALs were stained positive for all these three markers, although the membrane-associated markers (VMAT2 and DAT) showed weaker staining in the soma (Figure 5A). The neurotransmitter GABA was also detectable in iDALs, which is nonetheless consistent with a previous report showing that GABA is a co-transmitter in endogenous SNc DA neurons (Tritsch et al., 2012). In sharp contrast, iDALs did not express markers for other neuronal subtypes such as CHAT and VGLUT1.

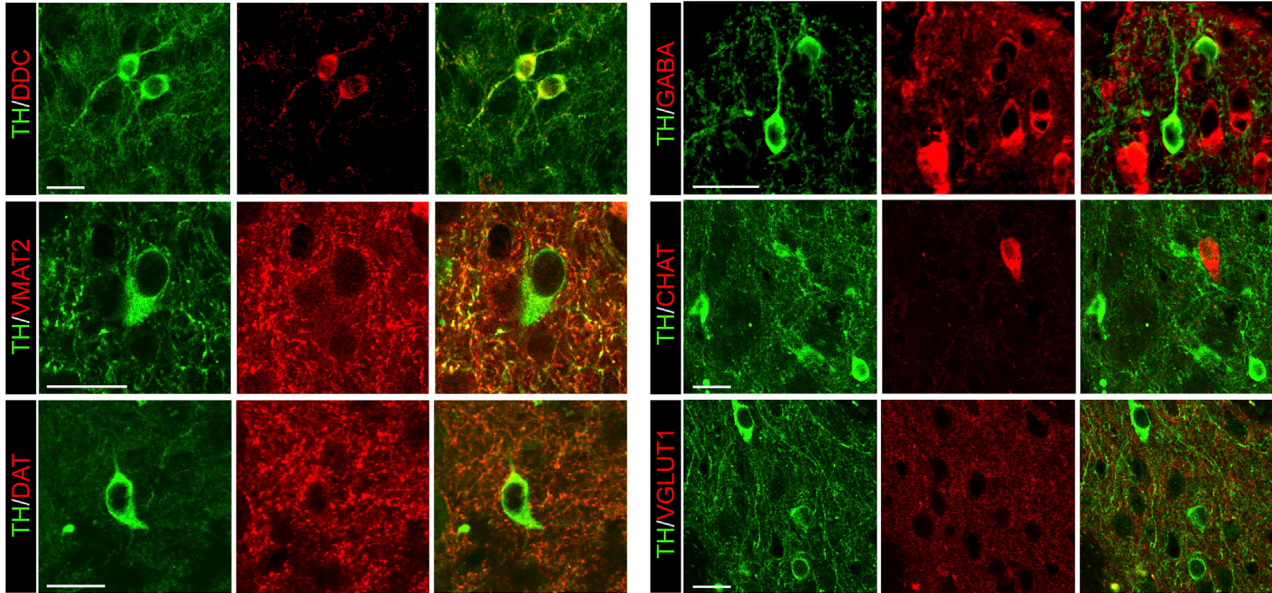
DAT staining in the cytosol of iDAL soma is weaker, which may reflect lower expression and membrane-bound localization. Its expression was then further confirmed in the *Dat-Cre;Rosa-tdT* reporter mice (Figure 5B), in which *IRES-Cre* was knocked into the endogenous *Dat* locus without disrupting its expression (Backman et al., 2006). TH⁺ DA neurons in the SNc were well labeled by the reporter tdT with strong soma expression (Figure 5B). Their axonal projections in the striatum were also tdT⁺. However, consistent with our TH-staining result, tdT⁺ somas were not observed in the core striatal regions under normal

Figure 4. Adult Striatal Neurons Are an Origin for iDALs

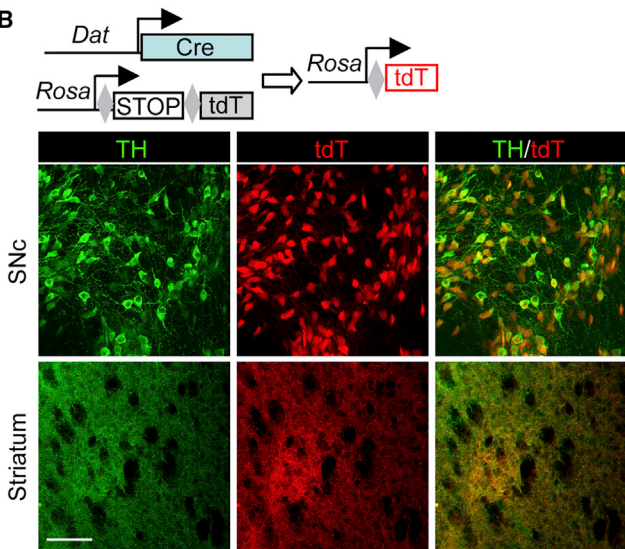
(A) iDALs come from endogenous neurons. Endogenous neurons and their derivatives were traced in *PrP-CreER^T;Rosa-tdT* mice after Tam injections (n = 206 tdT⁺TH⁺ cells out of 259 TH⁺ cells from three mice). TH⁺ iDALs are clearly labeled by the reporter tdT. Scale bar, 20 μm.
(B) iDALs retain expression of CTIP2, a marker for striatal neurons. DA neurons in SNc were used as controls. Scale bar, 20 μm.
(C) iDALs retain expression of DARPP32, a marker for striatal neurons. DA neurons in SNc were used as controls. Scale bar, 20 μm.
See also Figures S5 and S6.



A



B



C

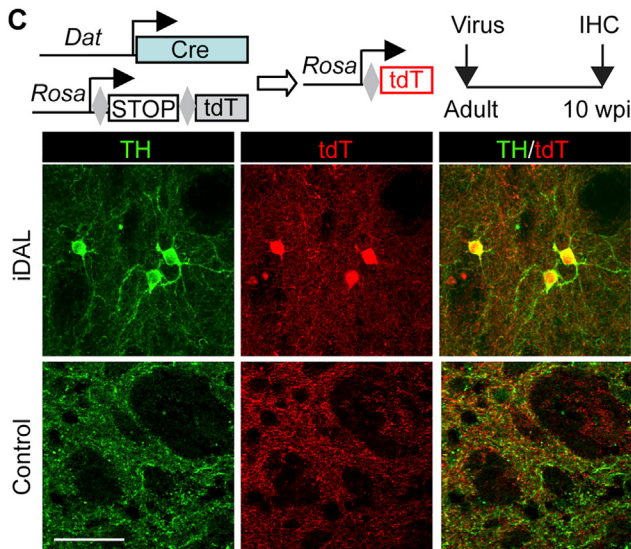


Figure 5. iDALs Express Markers for DA Neurons

(A) TH⁺ iDALs in the striatum express markers for DA neurons but not the other neuronal subtypes. Single-plane confocal images at 1 μm thickness are shown. Scale bar, 20 μm.

(B) A genetic approach to trace dopamine transporter-expressing cells. tdT⁺ somas were not observed in the core striatum, although numerous neuronal processes were clearly labeled in this region. Scale bar, 100 μm.

(C) Somas of iDALs but not endogenous striatal neurons are genetically labeled in *Dat-Cre;Rosa-tdT* reporter mice. Empty virus-injected brains were used as controls. Scale bar, 50 μm.

conditions (Figure 5B). These reporter mice were then injected with a control virus or iDAL factor-expressing virus (Figure 5C). When examined at 10 wpi, TH⁺ and tdT⁺ somas were detected in iDALs only in striatal regions injected with the iDAL factor-expressing virus but not a control virus (Figure 5C).

iDALs Possess Electrophysiological Properties Similar to DA Neurons

Through whole-cell patch-clamp recordings, we systematically analyzed the electrophysiological properties of iDALs in comparisons with endogenous neurons in the adult *Dat-Cre;Rosa-tdT* mice. iDALs in the striatum and DA



neurons in the SNC, ventral tegmental area (VTA), and hypothalamus (HTH) were specifically identified by the reporter tdT expression. MSNs, the predominant neuronal subtype in the adult striatum, were tdT⁻ and used as controls. Some of the patch-clamp recorded cells were also infused with biocytin during recordings for subsequent verification by immunohistochemistry (Figure S7).

All the recorded cells showed inward sodium currents and outward potassium currents under depolarizing voltages (Figure 6A). Trains of action potentials (APs) were observed upon step injections of depolarizing currents indicating neuronal maturation (Figure 6B). iDALs had a range of capacitance similar to DA neurons in the HTH but significantly different from neurons in the other brain regions (Figure 6C; n = 8–23 neurons per group; **p < 0.01; ***p < 0.001; ****p < 0.0001). The input resistance of iDALs was in general similar to that of endogenous DA neurons but not MSNs (Figure 6D; n = 8–23 neurons per group; ***p < 0.001). Furthermore, iDALs had similar resting membrane potentials to endogenous DA neurons, which were significantly different from those MSNs (Figure 6E; n = 8–23 neurons per group; ****p < 0.0001). Detailed analysis of AP spikes also revealed differences among these recorded cells. Especially, the AP threshold, AP amplitude, and maximum velocity of spike rise and decay for iDALs were significantly different from those of endogenous MSNs (Figures 6F–6J; n = 8–23 neurons per group; *p < 0.05; ***p < 0.001; ****p < 0.0001). iDALs had an AP half-width similar to SNC DA neurons and MSNs but quite different from those DA neurons in the VTA and HTH (Figure 6H; n = 8–23 neurons per group; ****p < 0.0001). Overall, iDALs exhibited similar intrinsic properties to DA neurons in different regions of the adult brain.

iDALs Exhibit Firing Patterns Stereotypical to DA Neurons

Dramatically different from striatal MSNs, iDALs fired spontaneous APs, very similar to endogenous DA neurons (Figure 7A). The spontaneous firing frequencies of iDALs were within the range of resident DA neurons (Figure 7B; n = 8–23 neurons per group; **p < 0.01; ***p < 0.0001). The interspike interval coefficient variation, which is an indicator of spike interval variability, was also similar between iDALs and endogenous DA neurons (Figure 7C; n = 8–23 neurons per group; ***p < 0.0001).

Hyperpolarization-activated cyclic nucleotide-gated channels are a major source for spontaneous AP firings (Chu and Zhen, 2010; Zolles et al., 2006). It can be assessed by hyperpolarization-activated cation current (I_h), which is a direct measurement of current in voltage-clamp mode with prolonged hyperpolarization (Figure 7D), or by the sag voltage in current-clamp mode (Figure 7E). MSNs lacked significant I_h although they had sag voltage (Figures

7F and 7G; n = 8–23 neurons per group; **p < 0.01; ***p < 0.0001). On the other hand, iDALs showed both I_h and sag voltage, resembling endogenous DA neurons in the SNC and VTA. Interestingly, DA neurons in the HTH lacks both I_h and sag voltage, suggesting that other channel activity may be responsible for their spontaneous firings.

iDALs Form Functional Connections with Other Neurons

Spontaneous synaptic currents were recorded to determine the network connectivity of iDALs. The frequency and amplitude of spontaneous postsynaptic currents (sPSCs) were comparable for iDALs and the other resident neurons including DA neurons and MSNs (Figures 7H–7J; n = 8–23 neurons per group). The sPSCs can be further separated into slow and fast events. The slow events have a rise-time over 2 ms, whereas the fast events have a rise-time equal to or less than 2 ms. These two events represent a crude separation of excitatory and inhibitory inputs to the recorded neurons, because excitatory synaptic inputs through the AMPA and NMDA receptors have a longer rise-time than those inhibitory inputs from the GABA receptors (Kumar et al., 2002; Soltesz and Mody, 1994). Interestingly, iDALs had a more similar proportion of slow and fast synaptic inputs to those resident DA neurons than MSNs (Figures 7K and 7L; n = 8–23 neurons per group; *p < 0.05). Together, these results indicate that iDALs are functionally mature and possess electrophysiological properties resembling endogenous DA neurons but not MSNs.

DISCUSSION

Expanding the repertoire of cells that can be phenotypically reprogrammed *in vivo*, the results of this study show that striatal neurons in the adult mouse brain can be converted to a phenotype resembling DA neurons. Properties of these iDALs are validated by genetic lineage tracing, marker expression, and, most importantly, extensive electrophysiological characterizations. Such results provide new perspectives on neuronal plasticity and cell identity maintenance.

DA neuron-like cells have been previously reprogrammed from cultured fibroblasts (Caiazzo et al., 2011). Nevertheless, the same combination of transcription factors (ASCL1, LMX1A, and NURR1) completely failed to convert striatal glia into DA neurons in the adult mouse brain (Pereira et al., 2017; Torper et al., 2015). Such results suggest that cell origin and/or microenvironment may play a major role in reprogramming. A recent study reported the generation of TH⁺ neurons from resident glia by using a different combination of factors after 6-hydroxydopamine (6-OHDA)-induced brain lesions (Rivetti di Val Cervo et al.,

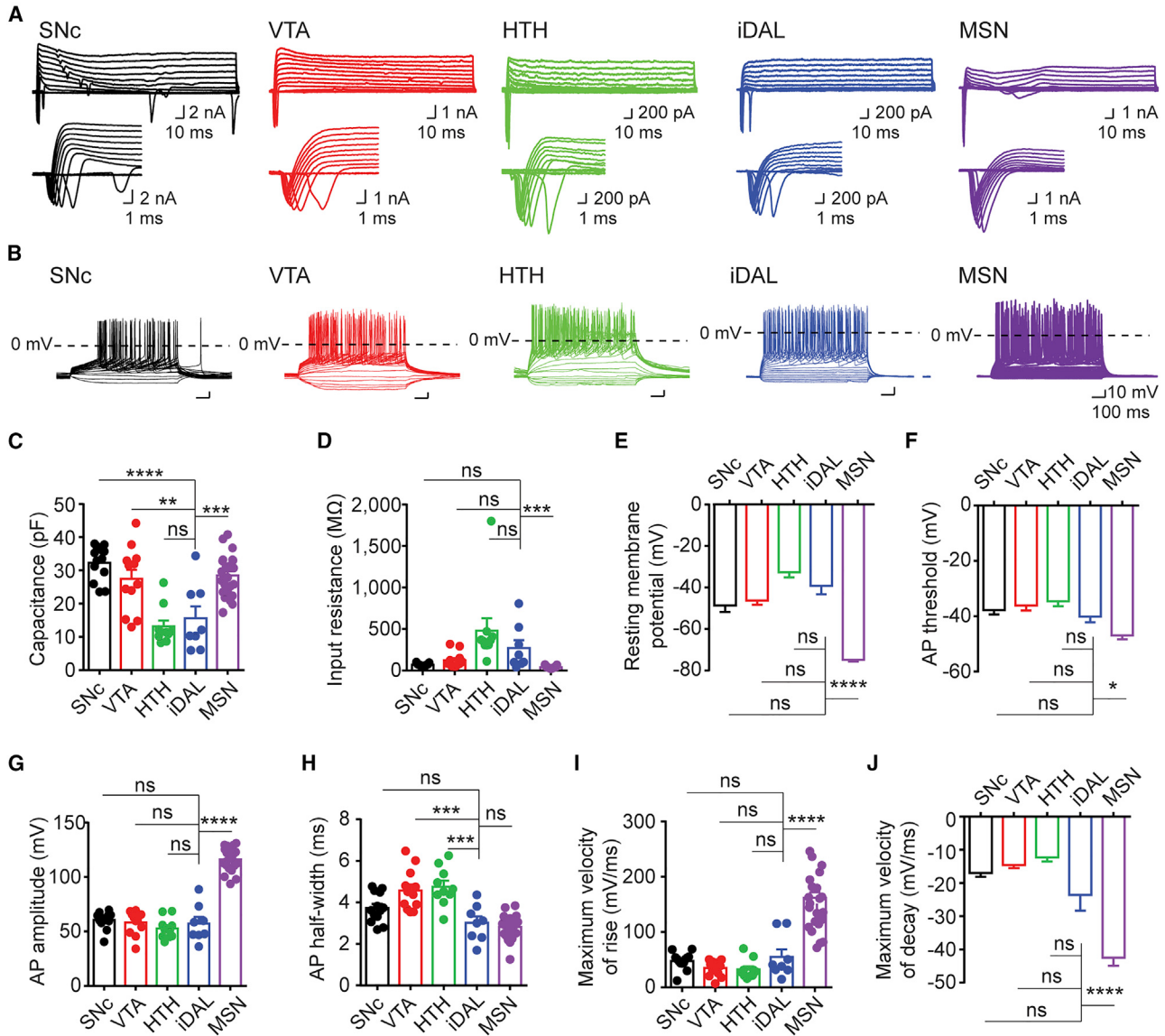


Figure 6. iDALs Exhibit Electrophysiological Properties Similar to DA Neurons

(A) Waveforms of inward and outward currents upon voltage steps. Whole-cell patch-clamp recordings were conducted on the indicated neurons. iDALs were analyzed at 8 wpi or later. The bottom panels are zoomed-in views of the waveforms. SNC, substantia nigra pars compacta; VTA, ventral tegmental area; HTH, hypothalamus; MSN, medium spiny neuron.

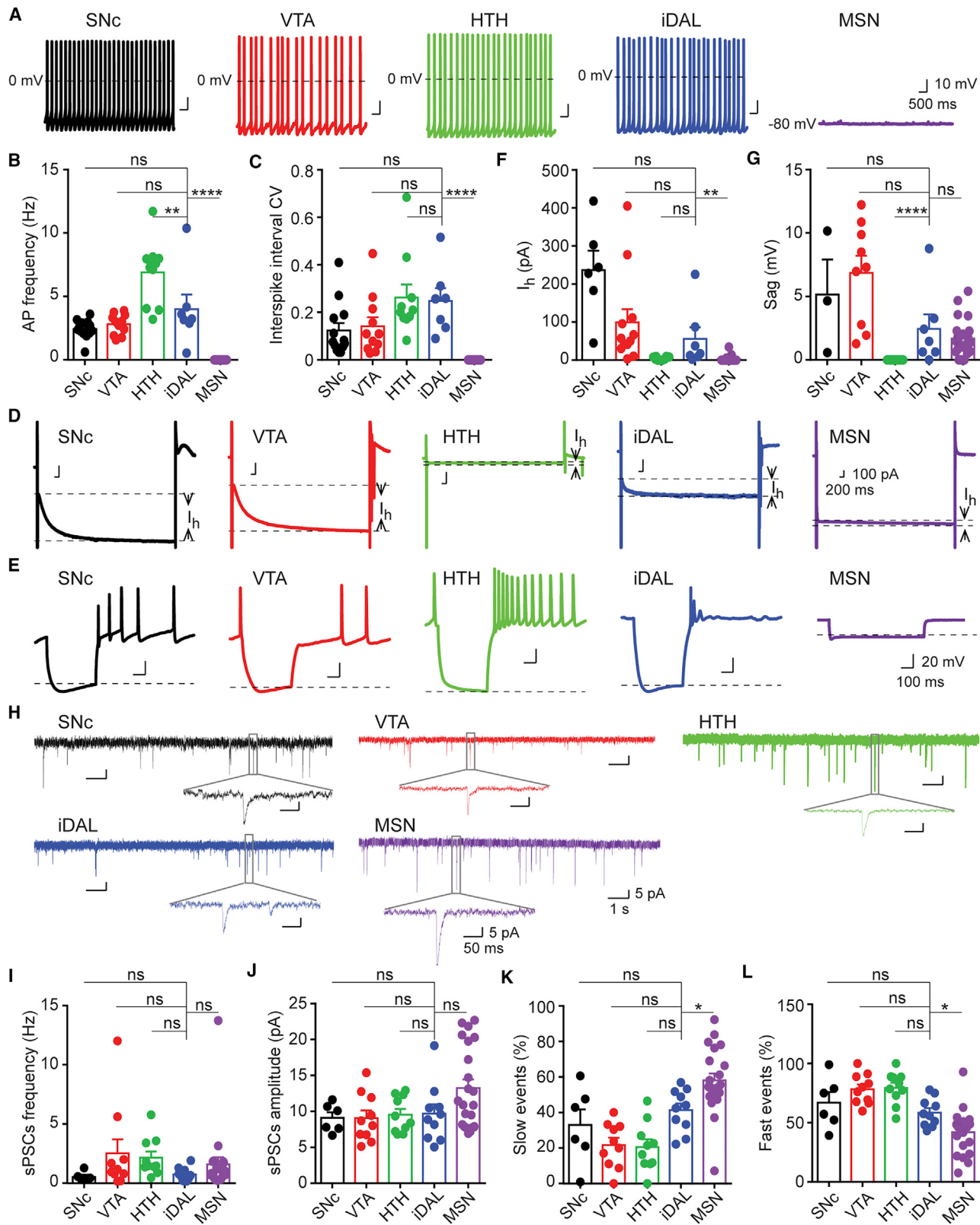
(B) Waveforms of action potentials upon current step injections.

(C–J) Intrinsic properties of the recorded neurons, including cell capacitance (C), input resistance (D), resting membrane potential (E), threshold potential (F), AP amplitude (G), spike width at half-maximal amplitude (H), maximum velocity of rise (I), and decay (J) of APs. iDALs but not MSNs resemble endogenous DA neurons (mean \pm SE; $n = 8$ –23 per group; * $p < 0.05$; ** $p < 0.01$; *** $p < 0.001$; **** $p < 0.0001$; ns, not significant; one-way ANOVA or Krushal-Wallis test with post hoc multiple comparisons).

See also Figure S7.

2017). However, the glial origin for those induced TH⁺ cells was uncertain since no well-established genetic reporter was employed, and the 6-OHDA lesion itself could induce the appearance of TH⁺ cells in the striatum (Pereira et al., 2017). Consistent with previous reports showing that TH⁺ cells were not detected in the adult mouse striatum

after various virus injections (Pereira et al., 2017; Torper et al., 2015), these cells were also rarely observed in our mice injected with control virus or treated with VPA. In this study, we initially aimed to identify conditions that could reprogram resident glia into DA neurons. After series of *in vivo* screens and systematic lineage mappings with



(legend on next page)



multiple genetic reporter lines, our results rather showed that neurons but not glia are the cell origin for our iDALs. Further studies are clearly needed to identify conditions that can reprogram resident glia into DA neurons.

Although iDALs could be induced by a combination of three DA neuron-restricted transcription factors (NURR1, FOXA2, and LMX1A), their number could be enhanced by the inclusion of SOX2 and VPA. VPA is a commonly used anti-convulsant and a histone deacetylase inhibitor with the ability to facilitate reprogramming of somatic cells to pluripotency (Huangfu et al., 2008). It can also promote neurogenesis through induction of *Neurod1* (Hsieh et al., 2004) and activation of the ERK signaling pathway (Hao et al., 2004). In this regard, ectopic *Neurod1* alone is sufficient to reprogram reactive glial cells to neurons (Guo et al., 2014), although VPA itself fails to induce any new neurons in non-neurogenic regions of the adult brain (Niu et al., 2013, 2015). Furthermore, VPA-induced BDNF expression may account for its ability to promote maturation and long-term survival of reprogrammed neurons in the adult mouse brain and spinal cord (Niu et al., 2013, 2015; Su et al., 2014). These multiple functions of VPA may be important for its role in the generation of iDALs.

It is currently unclear how a stem cell factor, SOX2, promotes phenotypic reprogramming of adult neurons *in vivo*. It has been previously shown that SOX2 exhibits intrinsic properties of a pioneering transcription factor that can target silent sites of nucleosomes to initiate cellular reprogramming (Soufi et al., 2015). Its binding to intractable genomic loci can be further enhanced by the ubiquitously expressed PARP1 in an enzymatic activity-independent manner (Liu and Kraus, 2017). Such pioneer activity of SOX2 may open up chromatin structure that is needed for further reprogramming by other fate-determining transcription factors, such as ASCL1 in pericytes (Karow et al., 2012) and DA neuron-restricted factors in neurons (this study). Because of its high expression in glial cells, ectopic

SOX2 may also have non-cell-autonomous effects that create a microenvironment facilitating phenotypic reprogramming of striatal neurons by other DA factors.

Postmitotic cortical neurons can be reprogrammed into a different subtype by a single transcription factor, FEZF2 (De la Rossa et al., 2013; Rouaux and Arlotta, 2013). However, this subtype reprogramming is restricted to embryonic and very early postnatal stage indicating a critical period of nuclear plasticity (Rouaux and Arlotta, 2013). In contrast, our results show that the reprogrammable period can be extended into the adult stage if an appropriate combination of factors is employed. Our extensive analysis reveals that iDALs exhibit electrophysiological properties of endogenous DA neurons, such as resting membrane potential, firing threshold and amplitude for action potentials, spontaneous AP firings, and the hyperpolarization-activated current (I_h). Nonetheless, immunohistochemistry reveals that some MSN-restricted markers, such as CTIP2 and DARPP32, can still be detected in these iDALs, despite the lack of MSN-like electrophysiology. Such a result suggests that a complete suppression of gene expression programs in the original cells may need additional factors, although their residual expression is apparently not sufficient to block the DA neuron-like properties of iDALs.

In conclusion, our results unexpectedly reveal that adult neurons can be phenotypically reprogrammed *in vivo*, providing additional insights into our knowledge on neuronal plasticity and cell identity maintenance. Such knowledge may one day be applied to devise therapeutic strategies for treating neurological diseases through reprogramming the phenotype of local neurons.

EXPERIMENTAL PROCEDURES

Animals

Strategies and methods for generating the following transgenic mice have been described: *mGfap-Cre* line 77.6 (Gregorian et al., 2009), *PrP-CreER^T* (Weber et al., 2001), *Pdgfra-CreER^T* (Kang

Figure 7. iDALs Show Firing Patterns Stereotypical to DA Neurons

- (A) Representative waveforms of spontaneous AP firing at resting membrane potential.
(B and C) Quantitative analysis of spontaneous APs, including their firing frequency (B) and coefficient of variation of interspike intervals (C) (mean \pm SE; n = 8–23; **p < 0.01; ****p < 0.0001; ns, not significant; one-way ANOVA or Krushal-Wallis test with post hoc multiple comparisons).
(D) Representative I_h -current waveforms of the recorded neurons.
(E) Representative waveforms of voltage sag.
(F) Amplitude of I_h currents activated by hyperpolarization (mean \pm SE; n = 6–23; **p < 0.01; ns, not significant; Krushal-Wallis test with post hoc multiple comparisons).
(G) Amplitude of voltage sags (mean \pm SE; n = 3–23; ****p < 0.0001; Krushal-Wallis test with post hoc multiple comparisons).
(H) Spontaneous postsynaptic currents (sPSCs). Zoomed-in views of single events are also shown.
(I–L) Quantitative analysis of sPSCs, including their frequency (I), amplitude (J), slow events (K), and fast events (L) (mean \pm SE; n = 6–22; *p < 0.05; ns, not significant; one-way ANOVA with post hoc multiple comparisons).

See also Figure S7.



et al., 2010), *Dat-Cre* (Backman et al., 2006), and *Rosa-tdTomato* (Ai14) (Madisen et al., 2010). Wild-type C57/BL6J mice were obtained from the Jackson Laboratories. All mice were housed under a 12-hr light/dark cycle and had *ad libitum* access to food and water in the UT Southwestern animal facility. No significant phenotypic differences were observed between male and female mice; thus, both genders were included in the analysis. Mice of ages 6 weeks to 24 months were used. Experimental protocols were approved by the Institutional Animal Care and Use Committee at UT Southwestern.

Virus Production and Stereotactic Brain Injections

The indicated human genes were subcloned into the CS-CDF-CG-PRE lentiviral vector. SOX2 was under the *hGFAP* promoter while the remaining factors were driven by the *hPGK* promoter. As described previously (Niu et al., 2013, 2015), replication-deficient lentivirus was produced in HEK293T cells after transient transfections. Virus was collected and concentrated by ultracentrifugation (25,000 rpm for 2 hr at 4°C) or polyethylene glycol precipitation. Striata of adult mice were stereotactically injected with a final volume of 2 µL virus each with an original titer of 0.5–2 × 10⁹ colony-forming units per mL. Viruses were mixed in equal volume for co-injection experiments. Injection coordinates are as follows: anterior/posterior, +1.0 mm; medial/lateral, ±2 mm; and dorsal/ventral from skull, –3.0 mm.

Tamoxifen, BrdU, and VPA Administration

Tamoxifen (T5648, Sigma) was dissolved in corn oil at a concentration of 20 mg/mL and injected intraperitoneally at a daily dose of 4 mg/40 g body weight for the indicated duration. Proliferative cells were labeled by BrdU (B5002, Sigma) through intra-peritoneal injections (100 mg/kg body weight, twice daily) or drinking water containing BrdU (1g/L) as indicated. VPA (P4543; Sigma) in drinking water (4 g/L) was administered for the indicated durations.

Immunohistochemistry and Quantification

Immunohistochemical analysis of 40-µm brain sections were conducted essentially as described previously (Niu et al., 2013, 2015). The following primary antibodies were used: BrdU (rat BU1/75, 1:500, Accurate Chemical), NeuN (MAB377, mouse, 1:500, Millipore), SOX2 (AB5603, rabbit, 1:500, Millipore), DCX (SC-8066, goat, 1:150, Santa Cruz Biotechnology), TH (chick, 1:1,000, Aves), DARPP32 (no. 2302, rabbit, 1:500, Cell Signaling Technology), CTIP2 (AB18465, rat, 1:500, Abcam), DAT (MAB369, rat, 1:200, Millipore), DDC (Ab3905, rabbit, 1:500, Abcam), VMAT2 (NBP1-69750, rabbit, 1:250, Novus), VGLUT1 (135311, mouse, 1:1,000, Synaptic), CHAT (AB144P, goat, 1:200, Chemicon), and GABA (A2052, rabbit, 1:500, Sigma). Alexa Fluor 488-, 594-, or 647-conjugated corresponding secondary antibodies from Jackson ImmunoResearch were used for indirect fluorescence. Images were taken using a Zeiss LSM510 confocal microscope. A Cell Counter software plugin in the ImageJ program was used to count cells. Data were obtained from one-sixth of the sections spanning the whole striatal region in each mouse. A representative image was shown from at least four similar ones. Confocal images

were Z series projections unless otherwise indicated in the figure legends.

Electrophysiology

Procedures were as described previously (Niu et al., 2013, 2015). In brief, acute midbrain slices were prepared for endogenous DA neurons and acute striatal slices were prepared for iDALS and MSNs. *Dat-Cre;Rosa-tdT* tracing line was used to trace DA neurons. For acute striatal slices, adult mice were deeply anesthetized and transcardially perfused with chilled striatal dissection buffer: 79 mM NaCl, 23 mM NaHCO₃, 68 mM sucrose, 12 mM D-glucose, 2.3 mM KCl, 1.1 mM NaH₂PO₄, 6 mM MgCl₂, 0.5 mM CaCl₂, and 1% kynureneate acid at pH 7.4, 300 mOsm, and aerated with 95%O₂/5%CO₂. The striatum with overlying neocortex was then dissected out. Acute sagittal slices (250 µm thickness) were collected between +2 and –2 mm from the bregma on a Leica VT1200S slicer. They were then incubated in aerated artificial cerebrospinal fluid (ACSF) containing 119 mM NaCl, 2.5 mM KCl, 26 mM NaHCO₃, 1 mM NaH₂PO₄, 11 mM D-glucose, 1 mM MgCl₂, and 2 mM CaCl₂ at pH 7.4, 300 mOsm, and aerated with 95%O₂/5%CO₂ to recover for 30 min at 35°C followed by additional incubation for over 1 hr at room temperature. For acute midbrain slices, the midbrain with attaching brain stem and cortex were dissected after anesthesia in chilled midbrain dissection buffer: 3 mM KCl, 1.25 mM NaH₂PO₄, 21 mM NaHCO₃, 10 mM D-glucose, 215 mM sucrose, 2 mM MgCl₂, 1.6 mM CaCl₂ at pH 7.4, 300 mOsm, and aerated with 95%O₂/5%CO₂. Midbrain slices (150 µm thickness) were then collected on a Leica VT1200S slicer. They were recovered in aerated ACSF at room temperature for at least 1 hr. In both cases, a single slice was then transferred to a submersion chamber and perfused at 3 mL/min with ACSF at 30°C for striatal slices and room temperature for midbrain slices. Lineage-traced cells in the striatum were identified under visual guidance using IR-DIC optics and tdT fluorescence. Whole-cell current-clamp and voltage-clamp recordings were performed using glass pipettes (4–7 MΩ) filled with intracellular solution: 0.2 mM EGTA, 130 mM K-gluconate, 6 mM KCl, 3 mM NaCl, 10 mM HEPES, 4 mM ATP-Mg, 0.4 mM GTP-Na, and 14 mM phosphocreatine-Tris at pH 7.2 and 285 mOsm supplemented with 0.5% Bio-cytin (B4261; Sigma). Biocytin-infused cells were detected with Alexa Fluor 488-conjugated avidin. All recordings were obtained with a MultiClamp 700B amplifier. Currents were filtered at 2 kHz, and acquired and digitized at 10 kHz using Clampex 10.3 (Molecular Devices). Both spontaneous and elicited APs were recorded in current-clamp mode; elicited AP was recorded by a series of current injections starting from –160 pA with 20, 40, 80, or 160 pA increments and 800 ms duration. Sag voltage was recorded in current-clamp mode with hyperpolarizing voltage steps from –60 mV with 10-mV intervals. *I_h* was recorded in voltage-clamp mode by injecting current to –130 mV and 6 s duration, and an average of 10 traces. Sodium and potassium currents were recorded in voltage-clamp mode in response to a series of voltage steps ranging from –60 to +60 mV at 10 mV increments and 100 ms duration. SPSCs were recorded in voltage-clamp mode. In all voltage-clamp recordings, cells were clamped at –60 or –80 mV, whichever was close to the resting membrane potential of the cell except during the voltage-step protocol. In all current-clamp



recordings, recordings were made at the resting membrane potential or without any current injection except otherwise stated. Series and input resistance were measured in voltage-clamp mode with a 400-ms, 10-mV step from a -60-mV holding potential (filtered by 10 kHz, sampled at 50 kHz). Cells were accepted only if the series resistance was less than 30 MΩ and stable throughout the experiment.

Data analysis was performed with Clampfit10.3 software (Molecular Devices). The AP trace immediately above threshold was used to determine the delay of the first spike as the length of time from the start of current steps to the peak of AP. The same AP trace was used to measure AP threshold as the corresponding voltage when there was the sharpest change of trace slope. The above-indicated AP trace was also measured to determine AP amplitude, half-width, and maximum velocity of rise and decay using the "Statistics" function from the "Analyze" menu as peak amplitude, half-width, and maximum rise and decay slope. AP frequency was obtained by dividing the maximum number of spikes during the current steps protocol with the step time duration (800 ms). Similarly, sodium and potassium currents were measured using the Statistics function. The biggest current was used. SPSCs were analyzed by using the Mini Analysis Program v6.0.7 (Synaptosoft). Traces were imported into the program, and baseline noise was measured by "measuring RMS noise" option in "Noise Analysis" menu. Four times the noise was used as the threshold for detection. Each individual event was carefully examined to avoid false positives. Statistics can be shown from the "Events" menus.

Statistical Analysis

All experiments were performed by using at least three mice per condition unless otherwise indicated. Statistics was done in GraphPad Prism. D'Agostino-Pearson omnibus normality test was first done on the data to determine whether it is a normal distribution. If the data passed the normality test, then one-way ANOVA was used to determine significance. If the data did not pass the normality test, then Krushal-Wallis test was used to determine significance. Significant differences are indicated by *p < 0.05, **p < 0.01, ***p < 0.001, or ****p < 0.0001.

SUPPLEMENTAL INFORMATION

Supplemental Information includes seven figures and can be found with this article online at <https://doi.org/10.1016/j.stemcr.2018.09.004>.

AUTHOR CONTRIBUTIONS

W.N., T.Z., and C.-L.Z. conceived and designed the experiments. W.N., T.Z., L.-L.W., and Y.Z. performed the experiments. W.N., T.Z., L.-L.W., and C.-L.Z. analyzed the data and prepared the manuscript.

ACKNOWLEDGMENTS

We thank members of the Zhang lab for discussions and reagents. We also thank J. Bibb and P. Chambon for providing *PrP-CreER^T* mice. C.L.Z. is a W.W. Caruth, Jr. Scholar in Biomedical Research. This work was supported by The Welch Foundation (I-1724), The Mobility Foundation, The Michael J. Fox Foundation (no. 9871),

The Decherd Foundation, The Pape Adams Foundation, the Texas Institute for Brain Injury and Repair, the Kent Waldrep Foundation Center for Basic Research on Nerve Growth and Regeneration, and NIH grants (OD006484, NS099073, NS092616, NS088095, and NS093502 to C.L.Z.).

Received: November 7, 2017

Revised: September 11, 2018

Accepted: September 13, 2018

Published: October 11, 2018

REFERENCES

- Arlotta, P., Molyneaux, B.J., Jabaoudon, D., Yoshida, Y., and Macklis, J.D. (2008). Ctip2 controls the differentiation of medium spiny neurons and the establishment of the cellular architecture of the striatum. *J. Neurosci.* **28**, 622–632.
- Backman, C.M., Malik, N., Zhang, Y., Shan, L., Grinberg, A., Hoffer, B.J., Westphal, H., and Tomac, A.C. (2006). Characterization of a mouse strain expressing Cre recombinase from the 3' untranslated region of the dopamine transporter locus. *Genesis* **44**, 383–390.
- Bond, A.M., Ming, G.L., and Song, H. (2015). Adult mammalian neural stem cells and neurogenesis: five decades later. *Cell Stem Cell* **17**, 385–395.
- Buffo, A., Vosko, M.R., Erturk, D., Hamann, G.F., Jucker, M., Rowitch, D., and Gotz, M. (2005). Expression pattern of the transcription factor Olig2 in response to brain injuries: implications for neuronal repair. *Proc. Natl. Acad. Sci. USA* **102**, 18183–18188.
- Caiazzo, M., Dell'Anno, M.T., Dvoretskova, E., Lazarevic, D., Taverna, S., Leo, D., Sotnikova, T.D., Menegon, A., Roncaglia, P., Colciago, G., et al. (2011). Direct generation of functional dopaminergic neurons from mouse and human fibroblasts. *Nature* **476**, 224–227.
- Chen, G., Wernig, M., Berninger, B., Nakafuku, M., Parmar, M., and Zhang, C.L. (2015). In vivo reprogramming for brain and spinal cord repair. *eNeuro* **2**. <https://doi.org/10.1523/ENEURO.0106-15.2015>.
- Chu, H.Y., and Zhen, X. (2010). Hyperpolarization-activated, cyclic nucleotide-gated (HCN) channels in the regulation of midbrain dopamine systems. *Acta Pharmacol. Sin.* **31**, 1036–1043.
- De la Rosa, A., Bellone, C., Golding, B., Vitali, I., Moss, J., Toni, N., Luscher, C., and Jabaoudon, D. (2013). In vivo reprogramming of circuit connectivity in postmitotic neocortical neurons. *Nat. Neurosci.* **16**, 193–200.
- Gascon, S., Murenu, E., Masserdotti, G., Ortega, F., Russo, G.L., Petrik, D., Deshpande, A., Heinrich, C., Karow, M., Robertson, S.P., et al. (2016). Identification and successful negotiation of a metabolic checkpoint in direct neuronal reprogramming. *Cell Stem Cell* **18**, 396–409.
- Grande, A., Sumiyoshi, K., Lopez-Juarez, A., Howard, J., Sakthivel, B., Aronow, B., Campbell, K., and Nakafuku, M. (2013). Environmental impact on direct neuronal reprogramming in vivo in the adult brain. *Nat. Commun.* **4**, 2373.
- Gregorian, C., Nakashima, J., Le Belle, J., Ohab, J., Kim, R., Liu, A., Smith, K.B., Groszer, M., Garcia, A.D., Sofroniew, M.V., et al.



- (2009). Pten deletion in adult neural stem/progenitor cells enhances constitutive neurogenesis. *J. Neurosci.* **29**, 1874–1886.
- Guo, Z., Zhang, L., Wu, Z., Chen, Y., Wang, F., and Chen, G. (2014). In vivo direct reprogramming of reactive glial cells into functional neurons after brain injury and in an Alzheimer's disease model. *Cell Stem Cell* **14**, 188–202.
- Hao, Y., Creson, T., Zhang, L., Li, P., Du, F., Yuan, P., Gould, T.D., Manji, H.K., and Chen, G. (2004). Mood stabilizer valproate promotes ERK pathway-dependent cortical neuronal growth and neurogenesis. *J. Neurosci.* **24**, 6590–6599.
- Heinrich, C., Bergami, M., Gascon, S., Lepier, A., Vigano, F., Dimou, L., Sutor, B., Berninger, B., and Gotz, M. (2014). Sox2-mediated conversion of NG2 glia into induced neurons in the injured adult cerebral cortex. *Stem Cell Reports* **3**, 1000–1014.
- Hsieh, J., Nakashima, K., Kuwabara, T., Mejia, E., and Gage, F.H. (2004). Histone deacetylase inhibition-mediated neuronal differentiation of multipotent adult neural progenitor cells. *Proc. Natl. Acad. Sci. USA* **101**, 16659–16664.
- Huangfu, D., Osafune, K., Maehr, R., Guo, W., Eijkelenboom, A., Chen, S., Muhlestein, W., and Melton, D.A. (2008). Induction of pluripotent stem cells from primary human fibroblasts with only Oct4 and Sox2. *Nat. Biotechnol.* **26**, 1269–1275.
- Jorstad, N.L., Wilken, M.S., Grimes, W.N., Wohl, S.G., VandenBosch, L.S., Yoshimatsu, T., Wong, R.O., Rieke, F., and Reh, T.A. (2017). Stimulation of functional neuronal regeneration from Muller glia in adult mice. *Nature* **548**, 103–107.
- Kang, S.H., Fukaya, M., Yang, J.K., Rothstein, J.D., and Bergles, D.E. (2010). NG2+ CNS glial progenitors remain committed to the oligodendrocyte lineage in postnatal life and following neurodegeneration. *Neuron* **68**, 668–681.
- Karow, M., Sanchez, R., Schichor, C., Masserdotti, G., Ortega, F., Heinrich, C., Gascon, S., Khan, M.A., Lie, D.C., Dellavalle, A., et al. (2012). Reprogramming of pericyte-derived cells of the adult human brain into induced neuronal cells. *Cell Stem Cell* **11**, 471–476.
- Kumar, S.S., Bacci, A., Kharazia, V., and Huguenard, J.R. (2002). A developmental switch of AMPA receptor subunits in neocortical pyramidal neurons. *J. Neurosci.* **22**, 3005–3015.
- Lee, Y., Messing, A., Su, M., and Brenner, M. (2008). GFAP promoter elements required for region-specific and astrocyte-specific expression. *Glia* **56**, 481–493.
- Lindvall, O., and Bjorklund, A. (2011). Cell therapeutics in Parkinson's disease. *Neurotherapeutics* **8**, 539–548.
- Liu, Z., and Kraus, W.L. (2017). Catalytic-independent functions of PARP-1 determine Sox2 pioneer activity at intractable genomic loci. *Mol. Cell* **65**, 589–603.e9.
- Liu, Y., Miao, Q., Yuan, J., Han, S., Zhang, P., Li, S., Rao, Z., Zhao, W., Ye, Q., Geng, J., et al. (2015). Ascl1 converts dorsal midbrain astrocytes into functional neurons in vivo. *J. Neurosci.* **35**, 9336–9355.
- Madisen, L., Zwingman, T.A., Sunkin, S.M., Oh, S.W., Zariwala, H.A., Gu, H., Ng, L.L., Palmiter, R.D., Hawrylycz, M.J., Jones, A.R., et al. (2010). A robust and high-throughput Cre reporting and characterization system for the whole mouse brain. *Nat. Neurosci.* **13**, 133–140.
- Niu, W., Zang, T., Zou, Y., Fang, S., Smith, D.K., Bachoo, R., and Zhang, C.L. (2013). In vivo reprogramming of astrocytes to neuroblasts in the adult brain. *Nat. Cell Biol.* **15**, 1164–1175.
- Niu, W., Zang, T., Smith, D.K., Vue, T.Y., Zou, Y., Bachoo, R., Johnson, J.E., and Zhang, C.L. (2015). SOX2 reprograms resident astrocytes into neural progenitors in the adult brain. *Stem Cell Reports* **4**, 780–794.
- Palmiter, R.D. (2008). Dopamine signaling in the dorsal striatum is essential for motivated behaviors: lessons from dopamine-deficient mice. *Ann. N. Y. Acad. Sci.* **1129**, 35–46.
- Pereira, M., Birtele, M., Shrigley, S., Benitez, J.A., Hedlund, E., Parmar, M., and Ottosson, D.R. (2017). Direct reprogramming of resident NG2 glia into neurons with properties of fast-spiking parvalbumin-containing interneurons. *Stem Cell Reports* **9**, 742–751.
- Rivetti di Val Cervo, P., Romanov, R.A., Spigolon, G., Masini, D., Martin-Montanez, E., Toledo, E.M., La Manno, G., Feyder, M., Pifl, C., Ng, Y.H., et al. (2017). Induction of functional dopamine neurons from human astrocytes in vitro and mouse astrocytes in a Parkinson's disease model. *Nat. Biotechnol.* **35**, 444–452.
- Rouaux, C., and Arlotta, P. (2013). Direct lineage reprogramming of post-mitotic callosal neurons into corticofugal neurons in vivo. *Nat. Cell Biol.* **15**, 214–221.
- Smith, D.K., and Zhang, C.L. (2015). Regeneration through reprogramming adult cell identity in vivo. *Am. J. Pathol.* **185**, 2619–2628.
- Smith, D.K., He, M., Zhang, C.L., and Zheng, J.C. (2016a). The therapeutic potential of cell identity reprogramming for the treatment of aging-related neurodegenerative disorders. *Prog. Neurobiol.* **157**, 212–229.
- Smith, D.K., Wang, L.L., and Zhang, C.L. (2016b). Physiological, pathological, and engineered cell identity reprogramming in the central nervous system. *Wiley Interdiscip. Rev. Dev. Biol.* **5**, 499–517.
- Soltesz, I., and Mody, I. (1994). Patch-clamp recordings reveal powerful GABAergic inhibition in dentate hilar neurons. *J. Neurosci.* **14**, 2365–2376.
- Soufi, A., Garcia, M.F., Jaroszewicz, A., Osman, N., Pellegrini, M., and Zaret, K.S. (2015). Pioneer transcription factors target partial DNA motifs on nucleosomes to initiate reprogramming. *Cell* **161**, 555–568.
- Su, Z., Niu, W., Liu, M.L., Zou, Y., and Zhang, C.L. (2014). In vivo conversion of astrocytes to neurons in the injured adult spinal cord. *Nat. Commun.* **5**, 3338.
- Torper, O., Pfisterer, U., Wolf, D.A., Pereira, M., Lau, S., Jakobsson, J., Bjorklund, A., Greish, S., and Parmar, M. (2013). Generation of induced neurons via direct conversion in vivo. *Proc. Natl. Acad. Sci. USA* **110**, 7038–7043.
- Torper, O., Ottosson, D.R., Pereira, M., Lau, S., Cardoso, T., Greish, S., and Parmar, M. (2015). In vivo reprogramming of striatal NG2 glia into functional neurons that integrate into local host circuitry. *Cell Rep.* **12**, 474–481.
- Tritsch, N.X., Ding, J.B., and Sabatini, B.L. (2012). Dopaminergic neurons inhibit striatal output through non-canonical release of GABA. *Nature* **490**, 262–266.
- Wang, L.L., and Zhang, C.L. (2018). Engineering new neurons: in vivo reprogramming in mammalian brain and spinal cord. *Cell Tissue Res.* **371**, 201–212.



- Wang, L.L., Su, Z., Tai, W., Zou, Y., Xu, X.M., and Zhang, C.L. (2016). The p53 pathway controls SOX2-mediated reprogramming in the adult mouse spinal cord. *Cell Rep.* **17**, 891–903.
- Weber, P., Metzger, D., and Chambon, P. (2001). Temporally controlled targeted somatic mutagenesis in the mouse brain. *Eur. J. Neurosci.* **14**, 1777–1783.
- Zhao, C., Deng, W., and Gage, F.H. (2008). Mechanisms and functional implications of adult neurogenesis. *Cell* **132**, 645–660.
- Zolles, G., Klocker, N., Wenzel, D., Weisser-Thomas, J., Fleischmann, B.K., Roeper, J., and Fakler, B. (2006). Pacemaking by HCN channels requires interaction with phosphoinositides. *Neuron* **52**, 1027–1036.

Supplemental Information

**Phenotypic Reprogramming of Striatal Neurons into Dopaminergic
Neuron-like Cells in the Adult Mouse Brain**

Wenze Niu, Tong Zang, Lei-Lei Wang, Yuhua Zou, and Chun-Li Zhang

Inventory of Supplemental Information:

Figure S1. Antibody specificity for TH staining in the adult mouse brain, related to Figure 1.

Figure S2. An in vivo screen to identify factors for inducing TH+ cells in the adult mouse striatum, related to Figure 1.

Figure S3. Genetic tracing of neuroblasts in the subventricular zone of adult mGfap-Cre;Rosa-tdT mice, related to Figure 3.

Figure S4. iDALs in injected striatal region far away from the lateral ventricle, related to Figure 3.

Figure S5. Tracing iDALs in the striatum of Prp-CreERT;Rosa-tdT mice, related to Figure 4.

Figure S6. Expression of viral SOX2 in striatal neurons and iDALs, related to Figure 4.

Figure S7. Verification of cell identity after patch-clamp recordings, related to Figures 6 and 7.

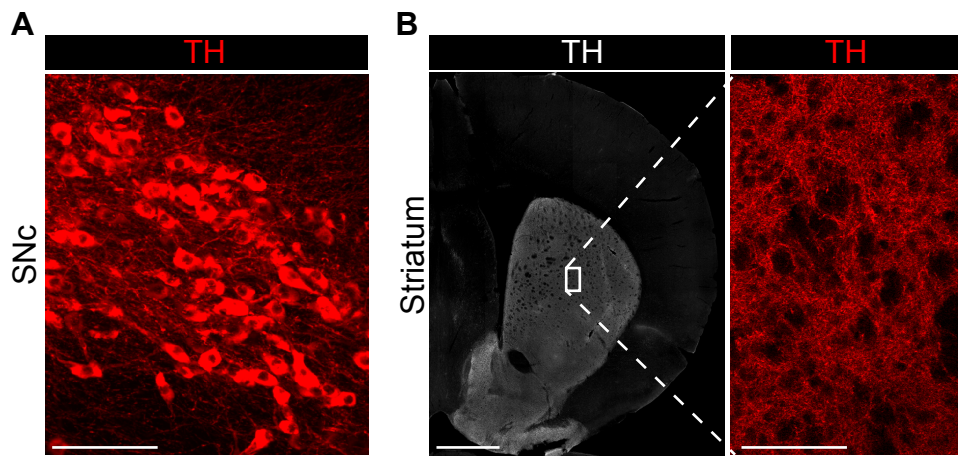


Figure S1. Antibody specificity for TH staining in the adult mouse brain, related to Figure 1.
(A) A representative image of TH⁺ neurons in the substantia nigra pars compacta (SNC). Neuronal somas and processes are clearly stained with the TH antibody. Scale bar: 100 μ m.
(B) TH⁺ neuronal processes in the striatum. No somas were stained with TH in the core striatum. Scale bars: 1.0 mm (in lower magnification view) and 100 μ m (in higher magnification view).

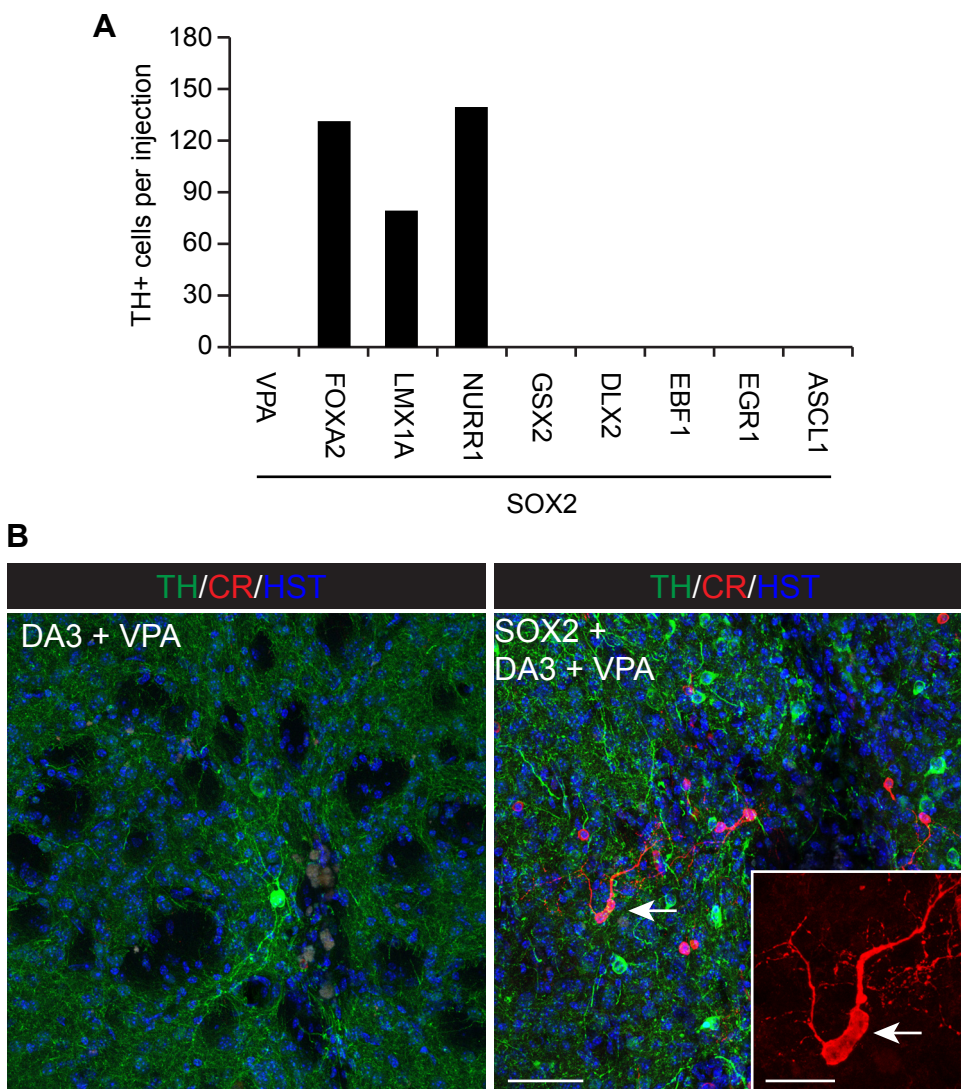


Figure S2. An in vivo screen to identify factors for inducing TH⁺ cells in the adult mouse striatum, related to Figure 1.

(A) TH⁺ somas were quantified at 8 weeks post virus injections in the adult mouse striatum (n=3-4 mice).
(B) Calretinin (CR)⁺ cells in the virus-injected striatal region. Scale bar: 20 μ m

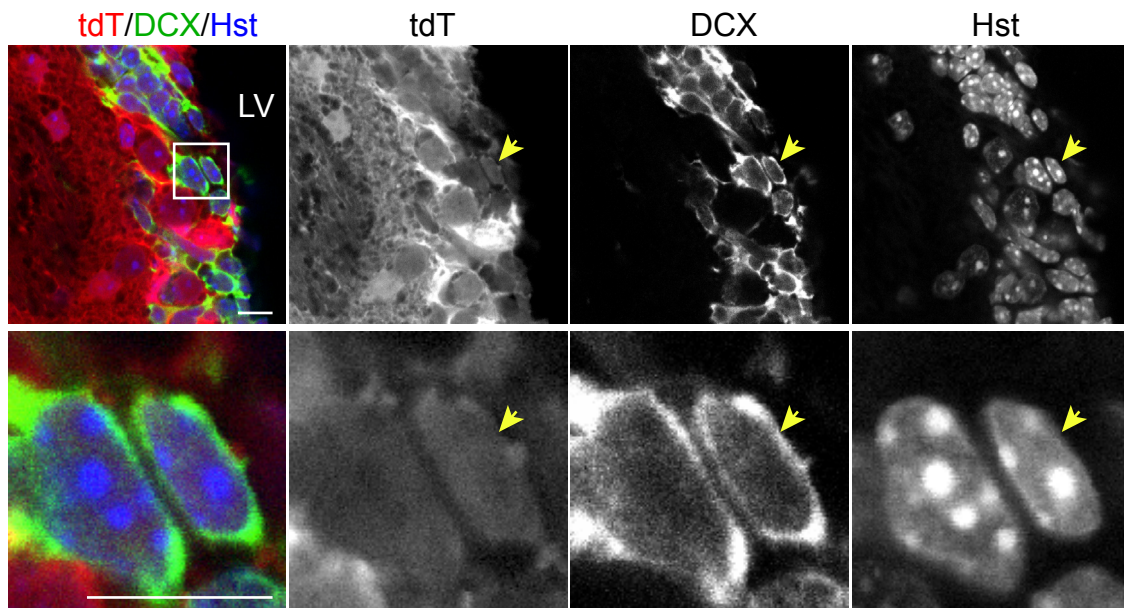


Figure S3. Genetic tracing of neuroblasts in the subventricular zone of adult *mGfap-Cre;Rosa-tdT* mice, related to Figure 3.

Neuroblasts in the subventricular zone were identified by DCX expression. Single-plane confocal images at 1- μm thickness are shown. Lower panel images are the enlarged views of the boxed region in the upper panel. The arrow indicates a typical tdT-traced neuroblast. LV, lateral ventricle. Scale bars: 10 μm

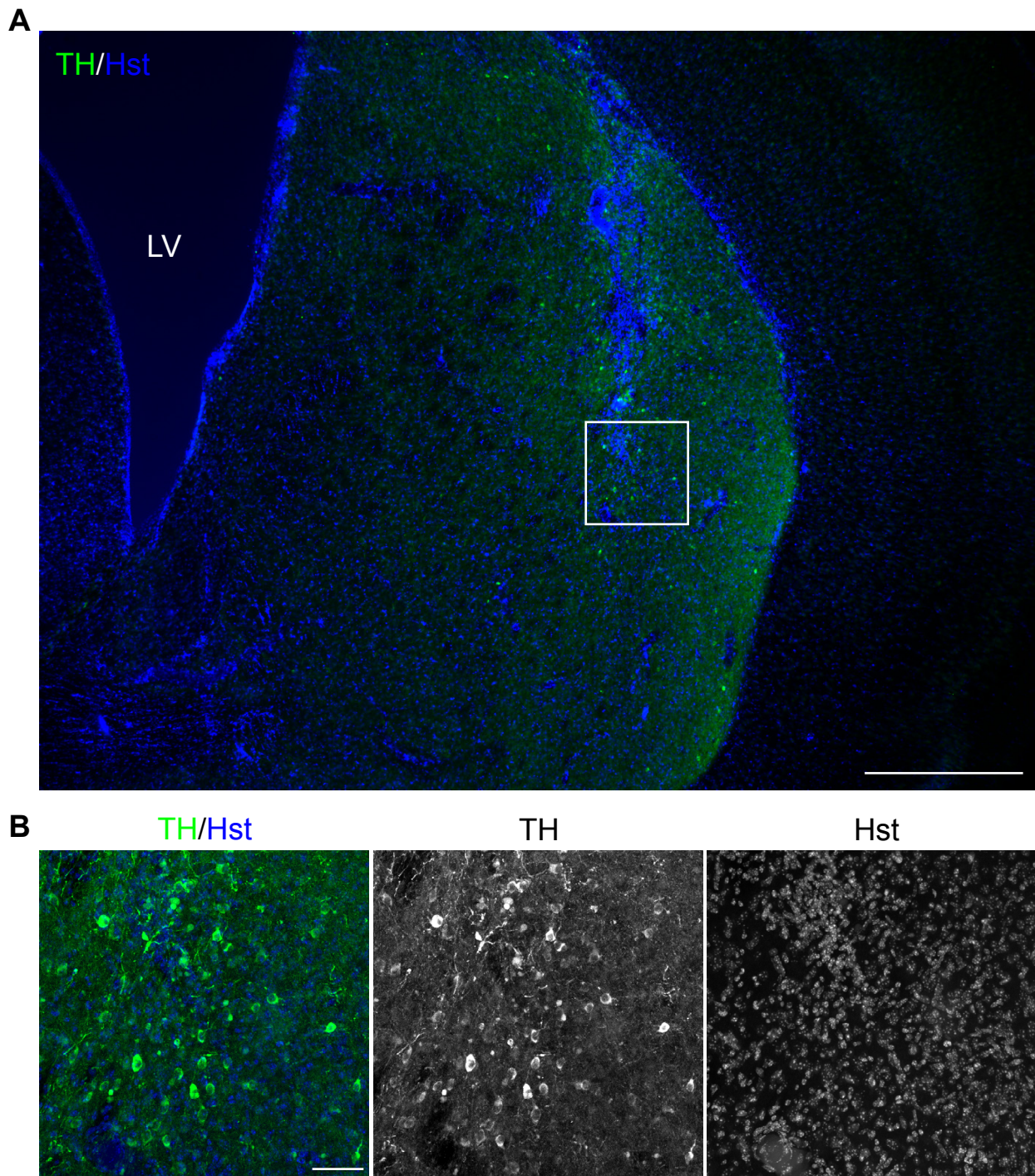


Figure S4. iDALs in injected striatal region far away from the lateral ventricle, related to Figure 3.
(A) A low magnification image of TH⁺ iDALs in the adult mouse striatum. These cells are detected in the virus-injected region far away from the lateral ventricle (LV). Scale bar: 1.0 mm.
(B) Zoomed-in confocal images of TH⁺ iDALs in the boxed region of panel A. Scale bar: 50 μ m.

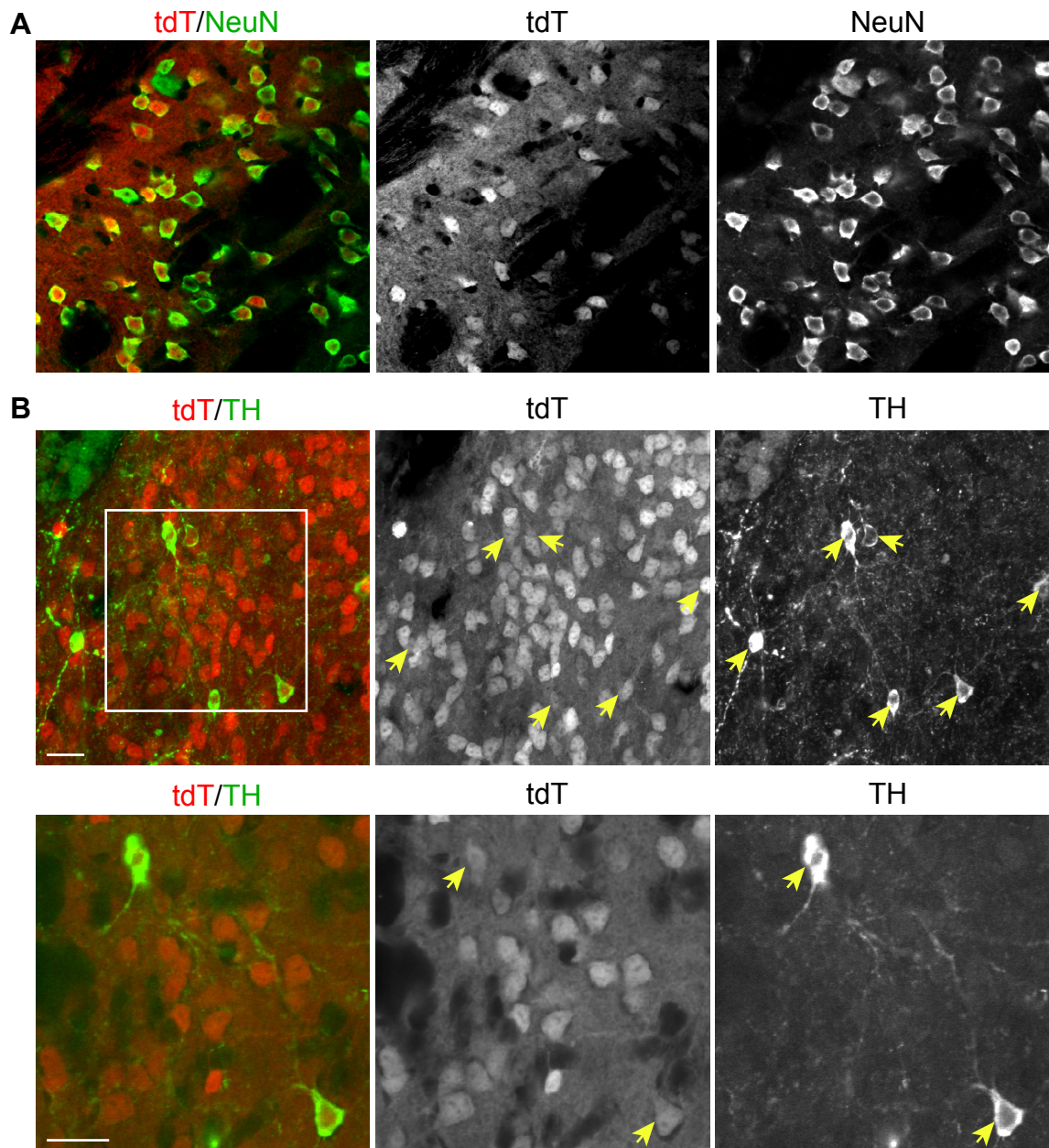


Figure S5. Tracing iDALs in the striatum of *Prp-CreER^T;Rosa-tdT* mice, related to Figure 4.

(A) Confocal images showing a majority of striatal neurons can be traced by tdT. Scale bar: 20 μ m.

(B) Additional confocal images showing tdT⁺ iDALs in the adult striatum. Single-plane confocal images at 1- μ m thickness of the boxed region in A are shown in the bottom panel. Scale bars: 20 μ m.

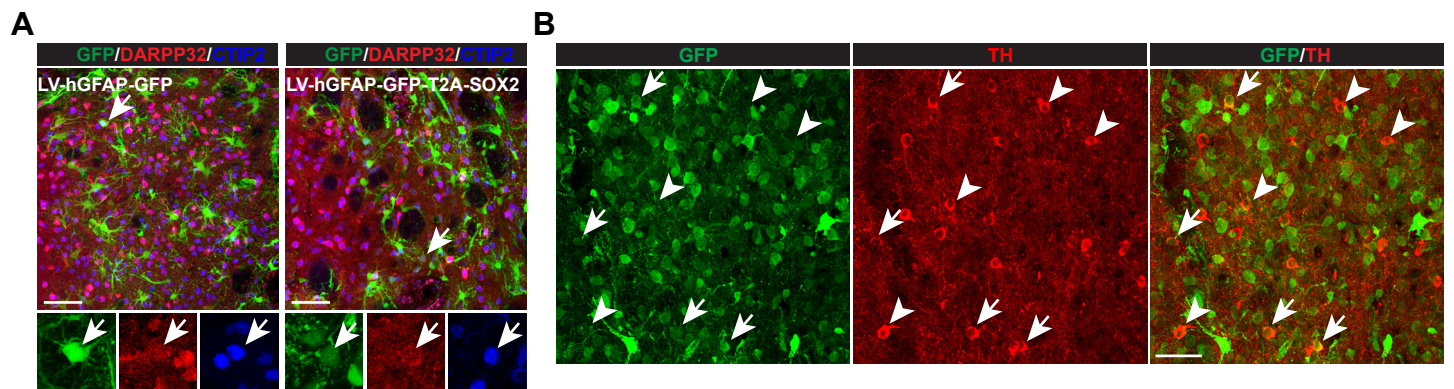


Figure S6. Expression of viral SOX2 in striatal neurons and iDALs, related to Figure 4.

(A) Lentiviral transduction of striatal neurons examined at 1 week post injection of virus. A representative neuron is indicated by an arrow.

(B) Expression of GFP-SOX2 in iDALs examined at 8 weeks post injection of viruses expressing GFP-SOX2, NURR1, FOXA2, and LMX1A. The mice were also treated with VPA in drinking water. Representative GFP⁺ iDALs are indicated by arrows, whereas GFP⁻ iDALs are shown by arrowheads. It should be noted that more neurons express the reporter GFP at this later time point.

Scale bars: 40 μ m.

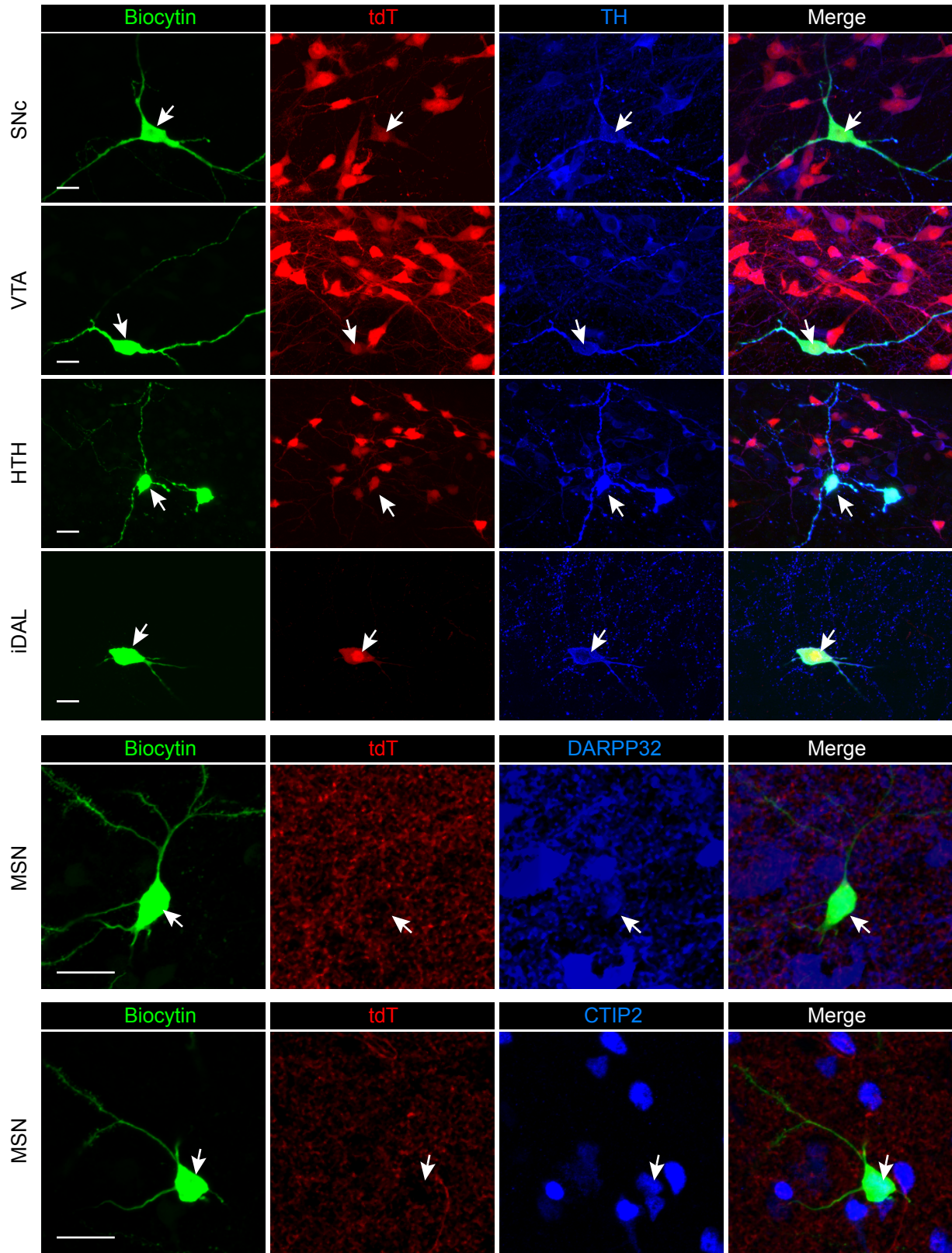


Figure S7. Verification of cell identity after patch-clamp recording, related to Figures 6 and 7.
 Some of the recorded neurons were infused with biocytin during recordings. iDALs in the striatum and endogenous DA neurons in the SNC, VTA, and HTH were traced in *Dat-Cre; Rosa-tdT* mice. Striatal MSNs are tdT-negative. Cell identities were further analyzed by immunohistochemistry with the indicated markers. Scale bars: 20 μ m.